JOURNAL OF NATURAL REMEDIES
DOI: 10.18311/jnr/2025/48209
RESEARCH ARTICLE

Investigating Anti-skin Aging Activity of Piperine-loaded Ethosomal Formulation in UV-B Induced Photoaging in Mice Model

Deepti Dwivedi[1], Nimisha Srivastava[1*], Neeraj Mishra[2], S. P. Singh[1] and Ankur Srivastava[3]

[1]Amity Institute of Pharmacy, Lucknow, Amity University Uttar Pradesh, Noida – 201313, Uttar Pradesh, India; nsrivastava3@lko.amity.edu

[2]Amity Institute of Pharmacy, Amity University Madhya Pradesh, Maharajpura, Gwalior – 474005, Madhya Pradesh, India

[3]Institute of Pharmacy, Dr. Ram Manohar Lohia Awadh University, Ayodhya – 224001, Uttar Pradesh, India

Abstract

Background: Premature dermal aging and wrinkles caused by Ultraviolet (UV-B) radiation can be characterised by collagen fragmentation, decreased dermal elasticity, and depleted epidermal thickness. **Aim:** Objective of the present research was to evaluate the skin aging activity of piperine-loaded ethosomes and compare it with marketed formulations. **Methods:** Ethosomes were prepared using the ether injection method. Twelve batches were prepared. The optimised formulations were lyophilised and incorporated into a 1% Carbopol base gel, and batch GF-5 gel showed the best results when characterised for spreadability, viscosity, drug content, etc. The probe-loaded optimised batch was visualised through Confocal Laser Scanning Microscopy (CLSM). The *in vivo* studies were performed on mice by initially inducing wrinkles and applying the locked formulation for 21 days on photo-aged mice skin. To evaluate the efficacy of the developed piperine formulation, the mice's skin was excised and observed through histopathological examinations, and Masson Trichome (M T) staining was also performed. **Results:** The prepared ethosomal vesicles ranged from 128.2±1.11 nm to 312.6±1.06 nm in size, and their Polydispersity Index (PDI) ranged from 0.107±1.21 to 0.322±1.32. The zeta potential (26.33 to -51.48 mV) confirmed the stability of the vesicles. The percentage entrapment efficiency ranged between 59±0.32 and 94±1.54, confirming proper piperine encapsulation into the ethosomes. *In vitro* permeation studies were performed, and batch F5 showed 85.87% drug release in 24 h. CLSM study showed a fluorescent intensity of 16.36 (at 30–40 µm) for probe loaded ethosomal formulation. Histopath images of excised mice's skin of GP 4 animals revealed improved collagen mass and fibroblasts. **Conclusion:** The research done for the ethosomal formulation of piperine showed an improvement in wrinkled skin. The formulation developed was found to be a safe, stable, convenient, and promising alternative to improve photo-aged skin conditions.

Major Findings: Piperine-loaded ethosomal gel was prepared and used against UV-B-induced photoaging. After 21 days of treatment, it confirmed the reduction of wrinkles, increased collagen synthesis, and fibroblast cells in the skin.

Keywords: Aging, CLSM, Ethosome, Photo-aged, Piperine, UV-B Radiation

Abbreviations: ANOVA : Analysis of Variance, , COA : Certificate of analysis, CLSM : Confocal Laser Scanning Microscopy , CPCSEA : Control and Supervision of Experiments on Animals; CYP : Cytochrome P, DLS : Dynamic light scattering , EE : Entrapment efficiency , ELS : Electrophoretic light scattering , FTIR : Fourier transform infrared, $GABA_A$: Gamma-aminobutyric acid type A; HES : Hydro-ethanolic solution, HPLC: High-performance liquid chromatography, HR-TEM: High-resolution transmission electron microscopy, IAEC:Institutional Animal Ethics Committee; IR : Infrared, KBr : Potassium bromide, MAO : Monoamine oxidase, MMP : Matrix metalloproteinase, MT Staining : Masson's trichrome staining, NF-κB : Nuclear factor-kappa B; NIPER : National Institute of Pharmaceutical Education and Research, PBS : Phosphate buffer solution, PDI : Polydispersity index, ROS : Reactive oxygen species; RPM : Revolutions per minute, SKU : Stock keeping unit, Soya PC : L-α-phosphatidylcholine, TEM : Transmission electron microscopy, TGF- β : Transforming growth factor beta, TNF-α : Tumour necrosis factor α; IL-1β : Interleukin-1β, UV radiations : Ultraviolet radiations

*Author for correspondence

Article Received on: 17.01.2025 Revised on: 25.03.2025 Accepted on: 23.04.2025

1. Introduction

The skin is the most extensive body organ in humans, enveloping a surface area of approximately meters. It makes up for a significant part of our body weight, roughly 15 %, and acts as a major sensory shield against environmental influences. The skin performs many tasks and competently protects us from UV rays, microorganisms, mechanical, osmotic, chemical, and thermal damage[1]. Skin changes are due to natural biological processes (intrinsic aging) and environmental influences (extrinsic aging)[2,3]. In the case of 'intrinsic aging', the basal cells' (epithelial progenitors) multiplication decreases, leading to gradual thinning of the epidermal layer and reduced nutritional exchange between the epidermis and dermis[4,5]. Both these occurrences are interrelated because a thinner epidermis further leads to less proliferation of the basal cells[6]. This moderate decline in proliferation also affects the augmentation of keratinocytes, melanocytes, and fibroblasts. Intrinsic aging also causes a decrease in elastin fibers, collagen production, the size of dermal fibroblasts, and the skin's hydration retention capacity[7,8]. The substantial alterations in the extracellular matrix protein – elastin cannot be replenished due to its inert characteristic, and any changes that happen to it are permanent. Therewithal, Matrix Metalloproteinase (MMP), specifically MMP-1, -3, and -9, starts targeting elastin for fragmentation, leading to reduced skin elasticity. Due to the heightened expression of MMPs, collagen undergoes increased fragmentation[9].

Apart from intrinsic aging, humans also encounter changes due to 'extrinsic aging'. One of the major exogenous reasons for skin aging is due to Ultraviolet (UV) rays. The skin gets exposed to UVA, UVB, and UVC radiations, and although UVC is filtered out by the ozone layer, UVA and UVB can penetrate Earth's atmosphere and reach the skin dermis. These radiations can instigate the production of Reactive Oxygen Species (ROS) by interacting with chromophores and photosensitizers. ROS can cause lipid, protein, and DNA damage[10]. They commence the activation of transcription factor AP-1 (activated protein 1), which further generates the degrading enzyme MMP-1, responsible for collagens' cleavage of collagens. MMP-3 and MMP-9 also accelerate the degeneration of collagen and cause a direct effect on the integrity of the dermis. The UVB rays are considered the most harmful UV radiation because they can induce nuclear factor-kappa B (NF-κB – responsible for stimulating the transcription of inflammatory cytokines), which can directly interact with the DNA to form pyrimidine photo products such as pyrimidine pyrimidone and cyclobutane pyrimidine dimmers[11]. This compound has been shown to stimulate the digestive enzymes produced by the pancreas and inhibit oxidation reactions caused by free radicals. Moreover, research shows piperine helps reduce inflammation in multiple autoimmune conditions, including intestinal inflammation, early-onset diabetes, arthritis, and cancer development. It exerts its effects through multiple mechanisms[12]. It triggers the transient receptor potential vanilloid type-1 receptor and alters the activity of GABAA receptors. Piperine blocks Monoamine Oxidase (MAO) enzymes at similar concentrations, specifically MAO-A and MAO-B. In addition to other natural compounds that have methylenedioxyphenyl substituents and piperine, the skin influences the activity of cytochrome P450 (CYP) isoforms[13]. It inhibits CYP3A species while increasing the expression of CYP1A and CYP2B in the liver.

Furthermore, piperine exhibits a biphasic effect on the activity of P-glycoprotein, a crucial efflux transporter[14]. *In vitro* studies have demonstrated the protective capabilities of piperine against oxidative damage and its ability to neutralise free radicals and inhibit ROS, which are known to contribute to cellular damage. *In vivo*, studies have shown that piperine can play an important role in mitigating the detrimental effects of oxidative stress[15].

It has also been studied to increase renovating growth factor beta (TGF- β), enhance collagen repair, and reduce the NF-κB (chain-enhancer of activated B cells) in rodent periodontal tissues[16]. In small doses, it can act as a protective agent against oxidative stress prompted by high-fat diets in rats[17]. Piperine is also known to decrease inflammatory markers like Tumour necrosis factor α (TNF-α) and cytokine interleukin-1β (IL-1β)[18]. However, its effects against UV-B-induced photoaging have yet to be studied. As potent and useful phytochemicals like piperine are, a major challenge still exists in incorporating them as an effective dosage form due to their low solubility[19].

However, incorporating these constituents in novel vesicle carriers, ethosomes, can tackle the low solubility, stability, and bioavailability issues. These soft, malleable vesicles can encapsulate diverse natural molecules, including hydrophilic, lipophilic, and high molecular weight herbal-sourced compounds. The involvement of ethanol enables ethosomes to efficiently deliver their cargo into the inner layers of the skin, making them a promising drug delivery system for various dermatological and transdermal penetration. The transdermal approach can add value to developing a more convenient dosage format[20-22]. Therefore, this research will demonstrate the development of a transdermal piperine ethosomal gel formulation effective against UV-B-induced photoaging.

2. Materials and Methods

Piperine was received as a gift sample from Sami-Sabina Groups, Bengaluru, India, for academic research and development purposes. The sample also came with its Certificate of Analysis (COA). L-alpha Phosphatidylcholine (60% egg yolk) was purchased from Sigma Aldrich. The other solvents used were of analytical grade.

3. Drug Identification

Drug identification of Piperine was done with HPLC chromatography. A stock solution was prepared by accurately weighing 10 mg of piperine and dissolving it in 10 mL of HPLC-grade methanol. This stock solution was then used to create a series of dilutions ranging from 10 µg/mL to 100 µg/mL, also using HPLC-grade methanol. The mobile phase comprised 0.1% formic acid (5:95; acetonitrile: water) and acetonitrile. HPLC analysis was conducted at a wavelength of 254 nm using a Shimadzu LC 2010C HT system equipped with a PDA detector and controlled by LabSolutions software. A volume of 10 µL was injected for each analysis. Separation was performed on a 250 mm × 4.6 mm C18 column with a particle size of 5 µm at a temperature of 30°C, following isocratic elution at a flow rate of 1.5 mL/min[23].

4. Drug-excipient Interaction

A drug excipient interaction study was investigated by using FTIR spectroscopy. Physical mixture was used in a 1:1 ratio for compatibility studies. Infrared (IR) spectra of the physical mixture containing the drug and excipients were obtained using a Fourier Transform Infrared (FTIR) Spectrophotometer with the Potassium Bromide (KBr) disc method. First, a baseline correction was performed using blank KBr pellets. To prepare the sample, 3 to 5 mg of the physical mixture of the drug and excipients was thoroughly mixed with 100-150 mg of KBr and then compressed using a pressure machine to form a thin, transparent pellet (approximately 1 mm in diameter). This pellet was placed in the IR compartment of the instrument and scanned over a wavenumber range from 4000 cm^{-1} to 400 cm^{-1}. The spectra were recorded at the Central Instrumentation Facility using Perkin Elmer Spectrum IR (Version 10.6.1) at NIPER, Raebareli, India[24].

5. Formulation of Piperine-loaded Ethosomes

Ethosomes were prepared by the ether injection method. Ethosomes were prepared by the modified cold method. The quantity of L-α phosphatidylcholine and piperine was taken in a beaker, and ethanol was added to it. The beaker was covered with parafilm to prevent evaporation of ethanol. The solution was stirred on a magnetic stirrer, and the water was added drop by drop with the help of a syringe at room temperature17. Stirring was continued for the next 15 min. Sonication was done for the next 5 min to reduce the size of the prepared vesicles. The dispersions were stored in the refrigerator[25].

6. Characterisation of Piperine-loaded Ethosomes

6.1 Morphology

All prepared batches were subjected to morphological examination at a magnification of 100X using a Columbus microscope. Photographic images of the vesicles were captured for visual documentation with an iPhone 15 camera. Optimised batch F-5 was further characterised using high-resolution transmission electron microscopy (HR-TEM) with a TECNAI 20G system. This advanced technique provides detailed visualisation of vesicles and comprehensive morphological characterisation across various

scales, which aids in the optimisation of the chosen nanocarrier[26].

6.2 Zeta Potential, Vesicle Size, and PDI - Polydispersity Index

Dynamic light Scattering (DLS) and Electrophoretic Light Scattering (ELS) techniques were employed to measure the zeta potential, vesicle size, and Polydispersity Index (PDI) using a Malvern Zetasizer Nano 6.01 instrument from CIMAP in Lucknow, India. The vesicles were assessed to determine which formulation exhibited the best colloidal stability and homogeneity[27,28].

6.3 Entrapment Efficiency

The ultracentrifugation technique was used to determine the Entrapment Efficiency (EE%) of the piperine-loaded ethosomal vesicles. Aliquots of the formulation were subjected to high-speed centrifugation for 30 min at 10,000 RPM and a temperature of 4°C using a REMI Cooling Centrifuge. This process allowed the lipid-based nanocarrier to sediment, while the unentrapped piperine remained in the aqueous supernatant. After centrifugation, the supernatant was carefully removed to isolate the unentrapped piperine. The sedimented vesicles were then suspended in 1 mL of a 0.1% (v/v) Triton X-100 solution and subsequently diluted with pH 6.8 Phosphate-Buffered Saline (PBS).

The following formula provides the total percentage of the drug successfully entrapped in the ethosomal vesicles[29].

$$EE\% = \frac{Amount\ of\ drug\ present\ in\ vesicles}{Total\ Drug} \times 100$$

6.4 *In Vitro* Diffusion Study

A custom-fabricated glass Franz diffusion cell apparatus, with a diffusion area of 2.54 cm^2, was utilised to determine the *in vitro* permeation of the formulation. A Dialysis Membrane-50 (SKU: LA, Himedia Lab Pvt. Ltd., Mumbai, India) was used as the diffusion barrier. This membrane was equilibrated in Phosphate-Buffered Saline (PBS) at pH 6.8 for 4 h to ensure saturation and minimise potential osmotic effects during the experiment[30].

After hydration, the dialysis membrane was used between the donor and receptor compartments. The ethosomal dispersion being studied was then introduced into the donor chamber. The receptor compartment was filled with PBS at pH 6.8. Continuous magnetic stirring was applied to the receptor medium to prevent the formation of an unstirred water layer, which could hinder diffusion[31].

To prevent evaporation the donor compartment was sealed with Parafilm®. At predetermined time points (0.5, 1, 2, 3, 4, 5, 6, 7, 8, 12, and 24 hours), 1 ml aliquots were withdrawn from the receptor phase and immediately replaced with an equal volume of fresh, pre-warmed PBS. The concentration of permeated piperine in each sample was quantified spectrophotometrically using a Shimadzu UV-1800 at a wavelength of 342 nm[32,33].

6.5 Release Data Analysis

The results obtained from the *in vitro* permeation study were assessed through mathematical modelling using various kinetic equations to understand the mechanisms governing the drug release from the ethosomal system. The cumulative percentage of drug release was analysed according to three primary kinetic models: Zero-Order Kinetics, First-Order Kinetics, and Higuchi Release Kinetics. The correlation coefficients (R^2) for each model were calculated, and the model with the highest R^2 value was determined to best illustrate the release kinetics[34].

6.6 Confocal Laser Scanning Microscopy (CLSM)

The ability of the prepared ethosomal system to penetrate the skin was visualised using Confocal Laser Scanning Microscopy (CLSM). The probe was incorporated into the lipid phase at a concentration of 0.03% (w/v), co-dissolving it with Soy Phosphatidylcholine (SPC) in a chloroform-methanol solvent system.

An ethosomal dispersion loaded with the probe was applied to the dorsal area of excised animal skin, which was mounted in the Franz diffusion cell and maintained at 37°C for 8 h. After the study, the skin was rinsed with distilled water to remove any residual formulation. The treated skin area was then sliced and sectioned using a LEICA microtome. These sections were analysed with a confocal microscope.

6.7 *Ex Vivo* Release Study

In the *ex vivo* permeation study, the dialysis membrane was replaced with mice skin, which was positioned

between the donor and receptor chambers with the stratum corneum side facing upward into the donor chamber[35].

7. Preparation of Ethosomal Gel

The gel base was prepared by dispersing a measured amount of Carbopol 934P, which had been soaked in distilled water overnight, at a concentration of 1% (w/w). Meanwhile, the piperine-loaded ethosomal aqueous dispersion was subjected to lyophilisation (Chist Alpha 1-2 L Plus), resulting in a yellowish powder. Based on high entrapment efficiency 94±1.54 (EE%), stable zeta potential (26.33 to -51.48 mV), low polydispersity index (0.107±1.21 to 0.322±1.32), and vesicle size (128.2±1.11) less than 300 nm four ethosomal batches (F-1, F-3, F-5, and F-6) were selected, and after lyophilization was incorporated into 1 % Carbopol base gel. The pH of resulting gel formulation was adjusted by drop wise addition of triethanolamine.

7.1 *In Vitro* Drug Permeation Study of Gel

The *in vitro* drug permeation studies were conducted using hydroethanolic solution (HES); ethosomal gels labelled GF-1, GF-3, GF-5, and GF-7; a conventional gel, which is a simple gel with piperine suspended in a Carbopol base; and a commercially available anti-wrinkle formulation, specifically Himalaya's anti-wrinkle cream. The *in vitro* analysis followed the same experimental methods detailed earlier in this paper[37].

8. Characterisations of Piperine-loaded Ethosomal Gel

8.1 pH

pH of piperine-loaded nano-ethosomal gel was determined, and this was done by using the digital RI-152-R pH meter[38].

8.2 Viscosity

The viscosity of piperine-loaded ethosomal gel was quantitatively assessed using a Brookfield DV-III ULTRA viscometer at 100 RPM with Number 06 spindle[39].

8.3 Texture

The texture analysis of the optimised ethosomal gel was conducted using a TA XT2 texture analyser[40].

8.4 Spreadability

The spreadability of the ethosomal gels was assessed by measuring the rate at which two slides, placed apart by the gel, slid apart under a constant weight (measured in g.cm/sec). Spreadability is inversely related to viscosity; therefore, a shorter time for the slides to separate indicates better spreadability. Higher spreadability means that less shear stress is needed to apply the gel effectively[41].

8.5 Drug Content

The drug content of the prepared gels was assessed by dissolving a precisely weighed quantity of gel (100 mg) in 5 mL of ethanol. A 1 mL aliquot of this solution was then transferred to a 50 mL volumetric flask, and appropriate dilutions were made using PBS (pH 6.8). The resulting solution was filtered through a 0.45 µm membrane to remove any particulates. Finally, the absorbance of the filtered solution was measured at a wavelength of 340 nm using a Shimadzu-1800 spectrophotometer[42].

8.6 Stability Studies

The piperine-loaded ethosomal gel was stored for one month at temperatures of 4°C and 25°C. To evaluate its physical stability, visual observations and measurement of pH was done. Any significant changes in pH throughout the storage period were used as indicators to assess the gel's chemical stability[43].

8.7 Statistical Analysis

The statistical analysis was conducted using one-way and two-way ANOVA in Microsoft Excel, with significance determined at $p \leq 0.05$.

8.8 Animal Study

The protocols designed for the experiment were reviewed and approved by the Institutional Animal Ethics Committee (IAEC) to ensure compliance with the guidelines set by the Committee for Control and Supervision of Experiments on Animals (CPCSEA) (2234/GO/Re/S/23/CCSEA, 22/JUN/2023).

Mice were selected for the animal study and randomly assigned to five different groups. The hairs from their dorsal region were removed using a skin-friendly hair removal cream instead of a razor to avoid any potential skin damage caused by shaving blades.

Group 1 served as the control group, where photoaging was not induced. In Groups 2 to 5, photoaging was induced through exposure to UV radiation, using an Ultra Vitalux 300 W Walton bulb (Germany) positioned 30 cm above the dorsal skin of the mice. To determine the Minimal Erythemal Dose (MED), the mice's skin was exposed to varying durations of UV radiation. Wrinkles caused by photoaging were induced by exposing the dorsal skin to MED three times weekly for 30 days.

After wrinkle induction, the treatment phase was initiated, as per the protocol, topical treatments (piperine loaded in Carbopol conventional gel to GP 3 and piperine loaded ethosomal gel to GP 4) were given two times daily for 21 consecutive days. Group 5 was given topical application of marketed formulation (Himalaya anti-wrinkle cream). After the study, the extent of photoaging was evaluated macroscopically by capturing high-resolution digital images of the dorsal skin[44].

8.9 Histopathology and MT Staining Studies for Photo-aging Activity

For histopathological and MT Stanning studies, granulation tissue samples were excised from the photoaging-induced wrinkle model on the 21st day after treatment. To preserve their tissue architecture and cellular morphology, the samples were immediately fixed in a 10% formalin solution for 24 h and then dehydrated through a series of ethanol-xylene solutions.

After dehydration, the samples were filtered and embedded in paraffin wax (melting point range 40-60 °C). Using a microtome, sections were cut to a thickness of 10 µm and rehydrated through a reverse alcohol-xylene series. Haematoxylin-eosin dye was applied to stain the slides for visualisation. Finally, the stained sections were examined under a light microscope, and representative photographs were taken from each slide to compare the microscopic features across different groups[45].

9. Results

9.1 Drug Identification of Piperine and Drug Excipient Interaction

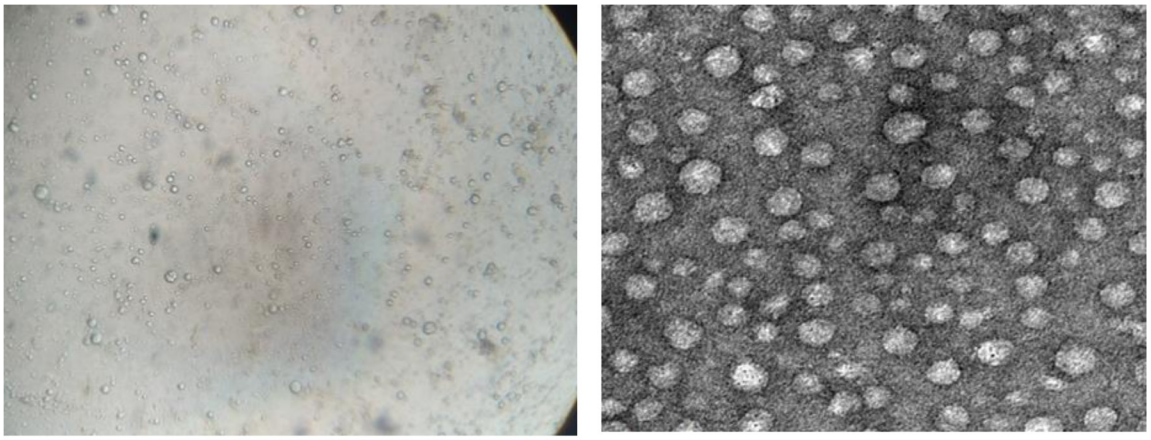
Drug identification has been done by using the HPLC method. Chromatograms of Piperine showed the highest peak at RT 17.50 min with the most prominent area. Drug excipient interaction studies were performed by using FTIR.

9.2 Characterisation of Ethosomes

Phase contrast and transmission electron microscopy were used to characterise the optimised batch (F5) morphologically, and images are given in Figure 1.

9.3 Vesicle Size, PDI, and Zeta Potential

The results of vesicle size, Polydispersity Index (PDI), and zeta potential are given in Table 1.



(a) **(b)**

Figure 1. **(a).** Phase contrast micrograph of optimised formulation (F5); **(b).** TEM micrograph of optimised formulation F5.

9.4 Entrapment Efficiency

This parameter indicates the proportion of the drug that was successfully incorporated into the vesicles, relative to the total amount of drug used during the formulation development process and the entrapment efficiency of all batches is given in Table 2.

9.5 *In Vitro* Permeation Study

Based on the zeta potential, PDI, vesicle size, and entrapment efficiency, batch F-1, F-3, F-5, F-6, and hydroethanolic solution were selected for the *in vitro* drug permeation study. Permeation studies for all the formulations were done for 12 h and graphs were plotted Cumulative % Drug Release vs time, Cumulative % Drug Release vs. square Root Time, and Cumulative % Drug Release vs. square Root Time which are shown in Figure 2, and the resulting R2 values were higher in zero-order than first-order (Table 3).

9.6 Confocal Laser Scanning Microscopy

An optimised batch F-5 was given for the confocal laser scanning microscopy, and results are shown in Figure 3, the bar graph was plotted between the penetration through the skin (µm) vs

Depth-wise visualisation:

- Thumbnails 1-6: 0-10 µm depth
- Thumbnails 7-12: 10-20 µm depth
- Thumbnails 13-18: 20-30 µm depth
- Thumbnails 19-24: 30-40 µm depth

9.7 Evaluation of Gel

All optimised ethosomal aqueous dispersions (F-1, F-3, F-5, and F-6) were lyophilised, and the powder was incorporated into the base gel. All the evaluation parameters of gel for the optimised batch were performed and tabulated in Table 4.

9.8 *Ex Vivo* Permeation Study

Ex-vivo permeation study of optimised formulations F-1, F-3, F-5, F-6, hydroalcoholic solution, the conventional and standard formulation was done for 24 h through mice skin and the graphs obtained from the study can be observed in Figure 4.

9.9 Photo-aging Activity

9.9.1 Wrinkle Induction

Wrinkles were induced in the mice for 21 days, and the images are shown in Figure 5.

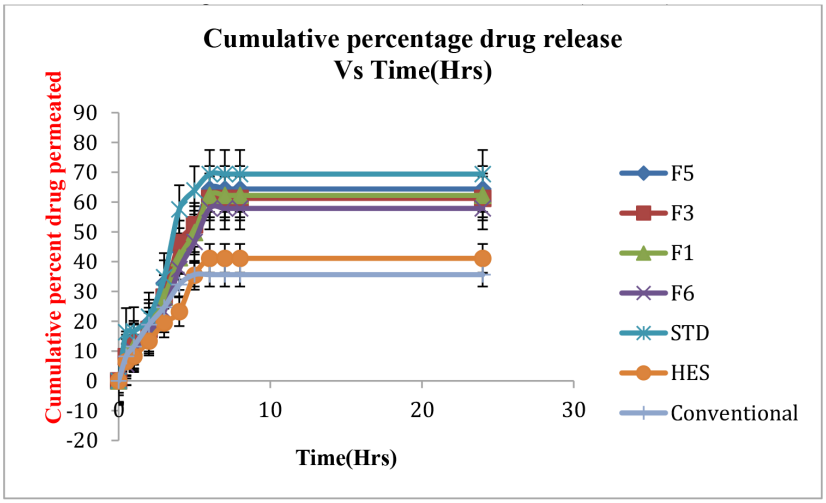
9.10 Histopathological Examination

Table 1. Vesicle size, PDI, and zeta potential of the ethosomal formulations

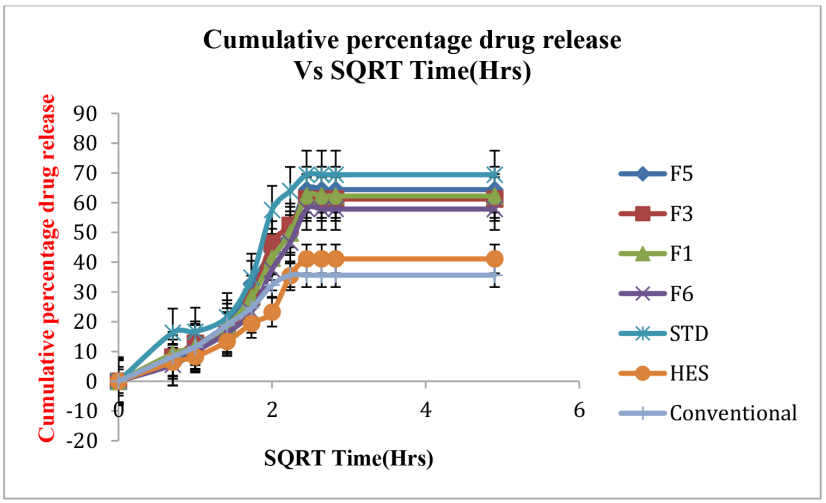
S. No.	Formulation code	Vesicle size (nm)	PDI	Zeta potential (mV)
1	F1	189.8±1.67	0.211±1.67	-28.45±1.17
2	F2	213.7±1.56	0.251±1.06	-26.67±1.05
3	F3	190.7±1.48	0.134±1.34	-23.67±1.14
4	F4	245.2±1.76	0.234±1.32	-45.32±1.10
5	F5	128.2±1.11	0.107±1.21	-26.33±1.07
6	F6	181.3±1.22	0.156±1.33	-29.56±1.11
7	F7	234.2±1.65	0.221±1.06	-29.19±1.21
8	F8	203.3±1.54	0.322 ± 1.32	-51.48±1.16
9	F9	232.6±1.67	0.267±1.45	-22.11±1.13
10	F10	256.2±1.87	0.284 ± 1.78	-36.34±1.08
11	F11	312.6±1.06	0.314 ± 1.43	-47.87±1.33
12	F12	245.5±1.87	0.298 ± 1.74	-43.67±1.66

Table 2. Entrapment efficiency (%) of the various ethosomal preparations

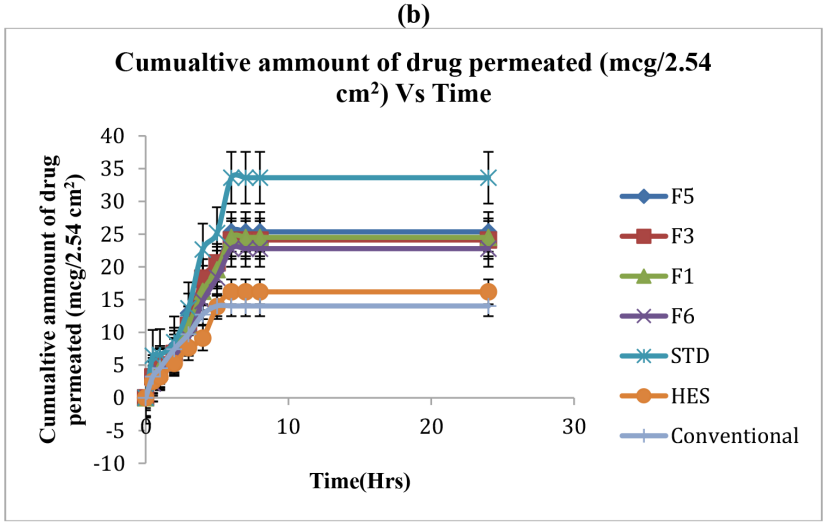
S. No.	Formulation code	Entrapment efficiency (%)
1	F1	93±1.23 (%)
2	F2	76±1.23 (%)
3	F3	91±0.06 (%)
4	F4	88±0.87 (%)
5	F5	94±1.54
6	F6	89±2.11
7	F7	76±1.21
8	F8	71±0.34
9	F9	65±1.06
10	F10	78±1.65
11	F11	59±0.32
12	F12	61±0.43



(a)



(b)



(c)

Figure 2. (a, b, c). Cumulative drug release after 24 h of optimised ethosomal formulation, conventional formulation, hydroethanolic solution, and standard formulation by cellophane membrane

9.11 Masson's Trichrome - MT Staining

Table 3. *In vitro* release results

Formulation ID	R^2 values		
	Zero-order	First order	Higuchi's
F1	0.9843	0.9691	0.9112
F3	0.9898	0.9754	0.9213
F5	0.9937	0.9638	0.9187
F6	0.9845	0.9895	0.9243

10. Discussion

This research study is designed to evaluate the anti-aging potential of piperine-loaded ethosomal gel. In this context, using piperine within an ethosomal system provides an innovative paradigm to treat photoaged skin. The dermal extracellular matrix stays in a perpetual homeostatic state through concurrent degradation and repair of the key structural units of the skin. However, the progression of skin aging can lead to pronounced modifications in the external appearance and textural

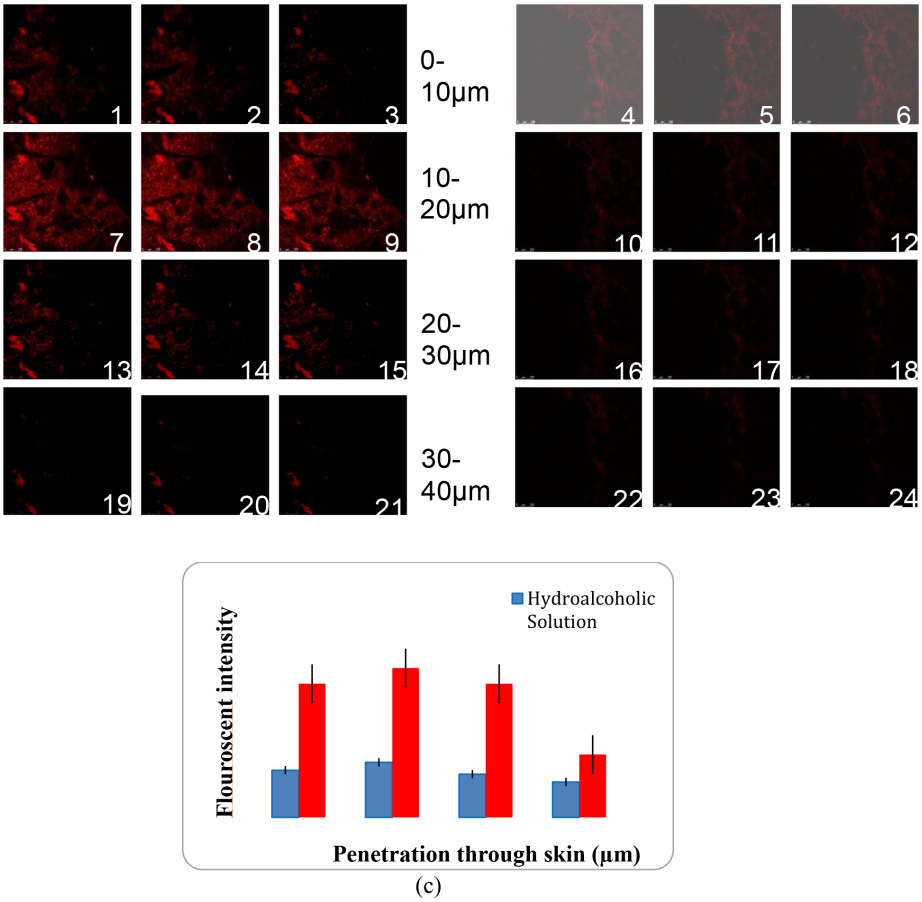
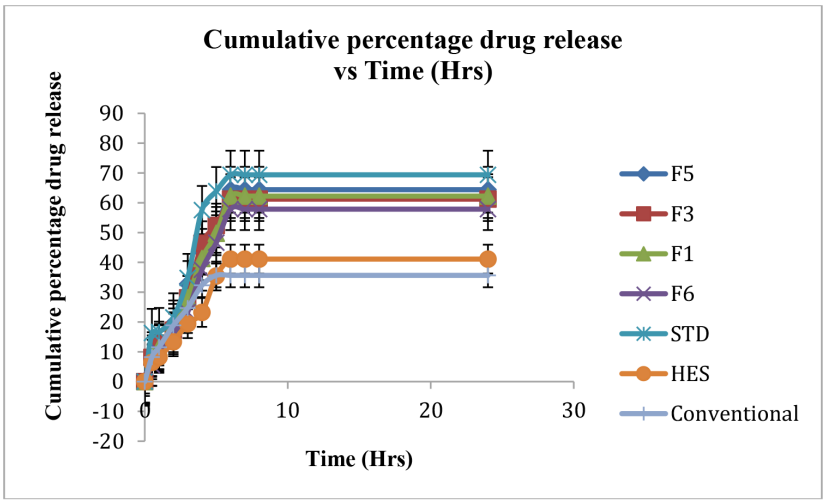


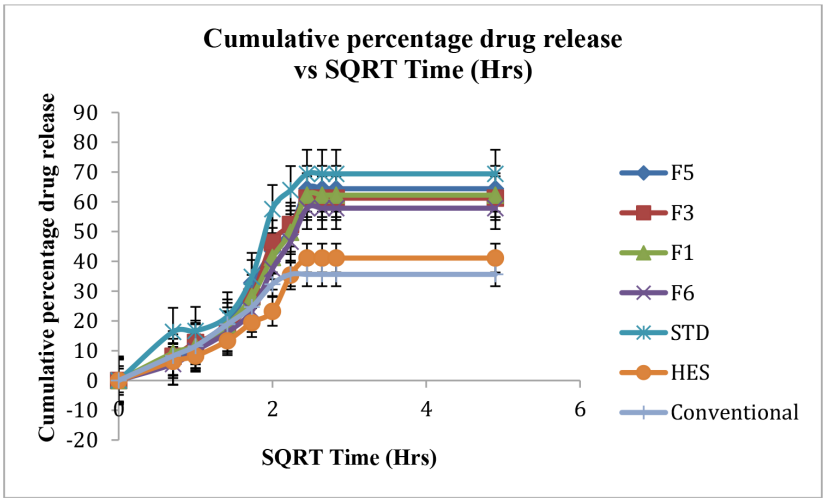
Figure 3. Fluorescent probe infiltration into mice skin - visualised through confocal microscopy. **(a).** Ethosome-encapsulated probe penetration, **(b).** Probe penetration in hydroalcoholic solution, **(c).** Probe's fluorescence intensity profile in mice skin.

Table 4. Characterisation of piperine-loaded ethosomal gel

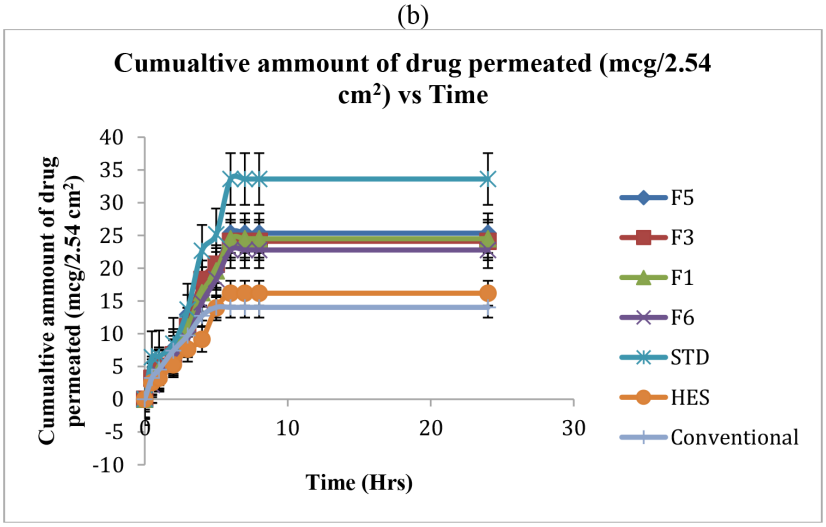
Formulation	Colour	Appearance	Spreadability (g.cm/s)	Viscosity (cps)	Drug content	pH
GF-1	Yellowish	Homogeneous	34.07±0.72	5200	73.65±1.4	7.05±0.03
GF-3	Yellowish	Homogeneous	33.03±0.56	6300	78.65±1.9	7.1±0.01
GF-5	Yellowish	Homogeneous	35.1±0.71	6600	81.47±1.4	6.7±0.07
GF-6	Yellowish	Homogeneous	32.07+0.26	5500	77.04±2.2	6.9±0.06



(a)



(b)



(c)

Figure 4. **(a, b, c).** Cumulative drug release after 24 h of optimised ethosomal formulation, conventional formulation, hydroethanolic solution, and standard formulation through mice skin.

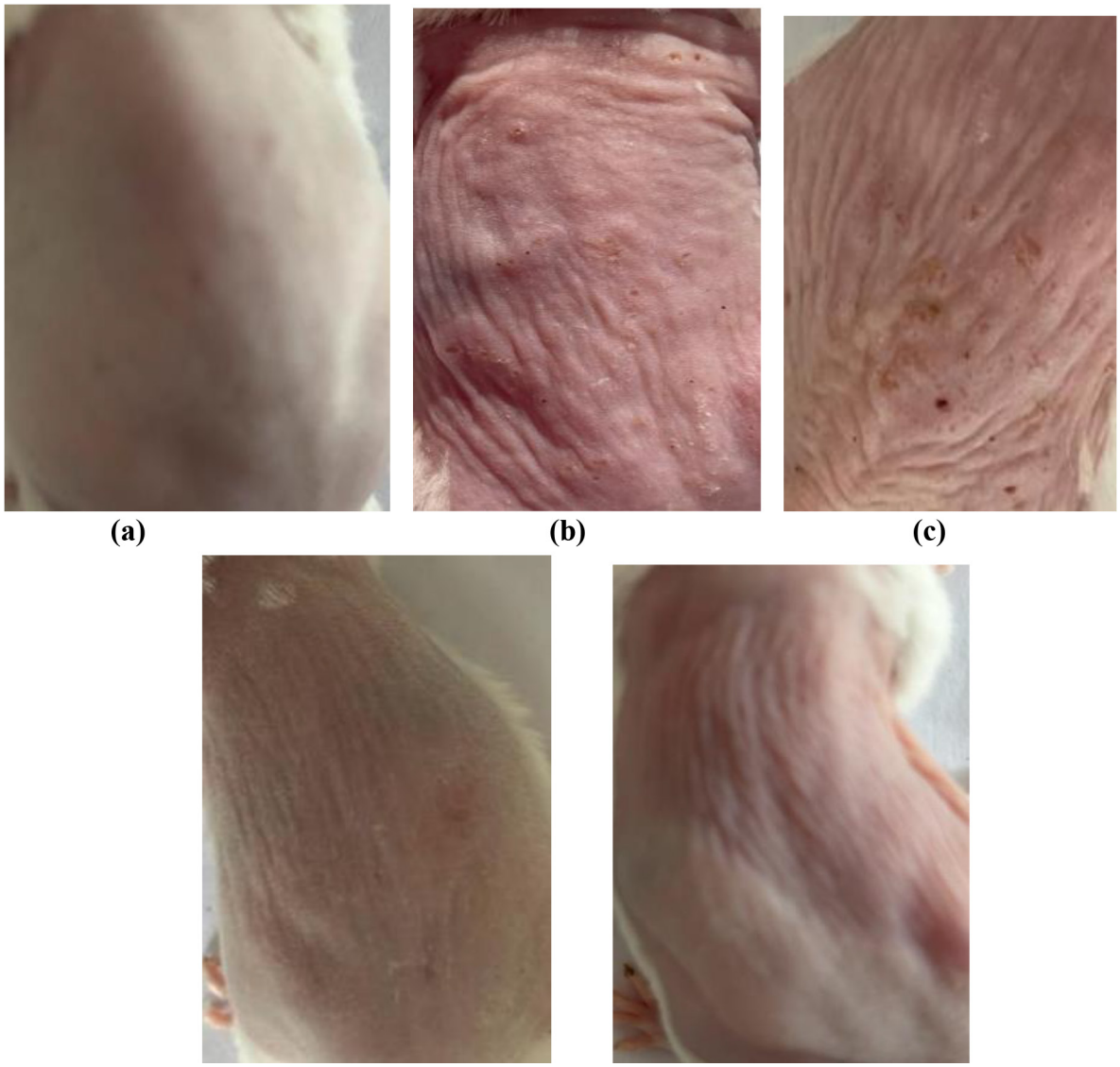


Figure 5. Photographic assessment of six different groups after the 21 days of treatment where **(a).** Normal Control Group, **(b).** Disease induced, **(c).** Conventional gel of piperine, **(d).** Ethosomal gel of Piperine, **(e).** Marketed formulation.

properties of the body's integument. To mend the changes caused due to skin aging, many naturally occurring actives are being researched continuously, and employing them transdermally can substantially restore aged dermal and epidermal structures. There has been remarkable research that has reported significant effects of piperine. The identification test for piperine was done using HPLC. The chromatogram of piperine showed a Retention time of 17.13. The presence of a specific peak for piperine at a retention time of around 17.12 was verified and thought to be a positive result for piperine. The opted active piperine was also compared with its standard through HPLC analysis, and the results showed that the sample had a prominent peak without any significant interferences.

In the drug excipient incompatibility study using FTIR, piperine showed the characteristic peak at 3252.89 corresponding to N-H stretching, 2923.85 corresponding to C=O stretching, soya PC showed a peak at 2924.16 corresponding to O-H stretching, and 1234.26 showed C-O-C stretching. All these peaks were present in the physical mixture of piperine and L-alpha phosphatidylcholine. No new peak generation confirmed, no incompatibility issue between the drug

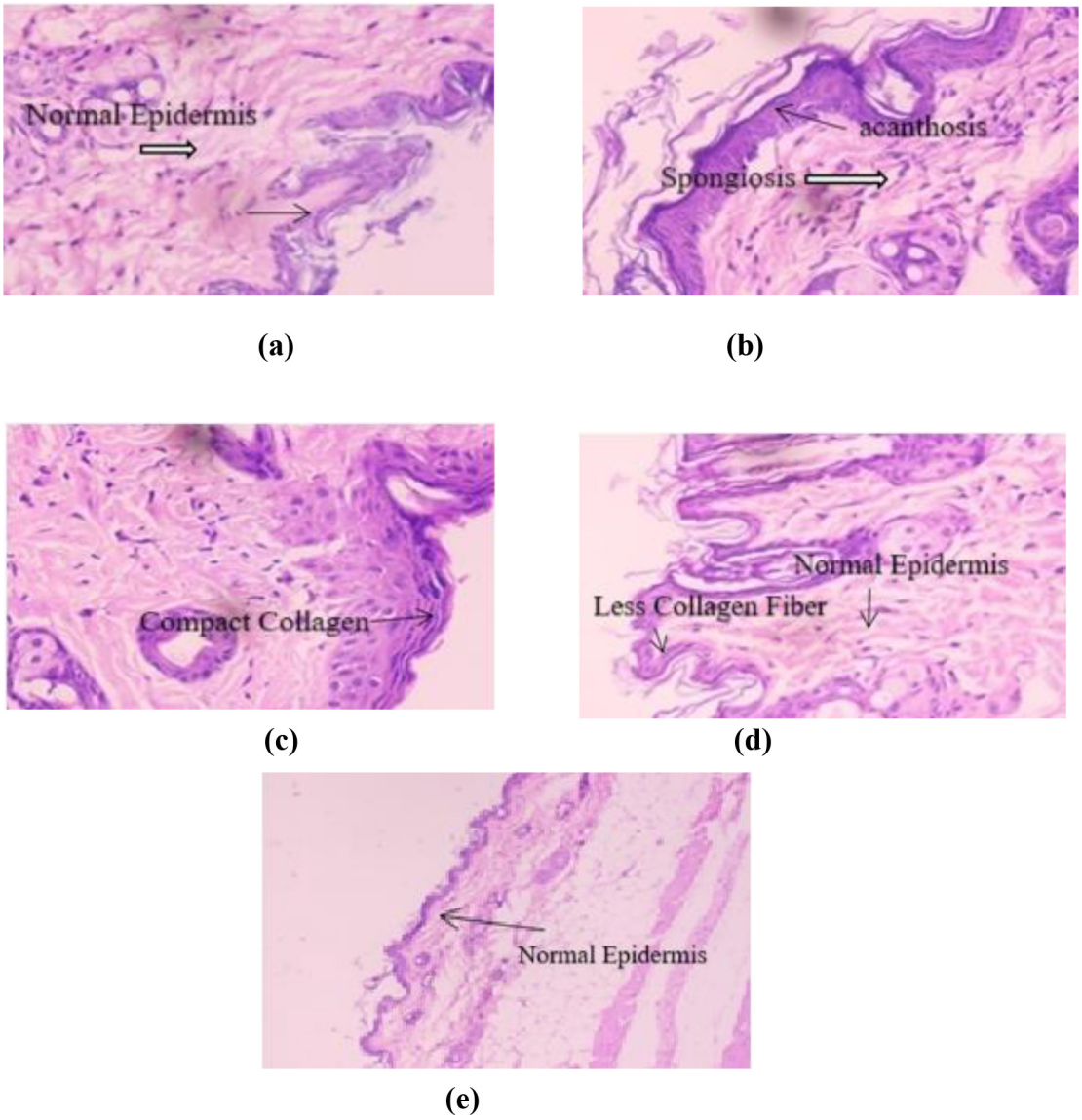


Figure 6. **(a).** Normal control animal showing (arrow) and dermal structure (arrowhead). (H. and E. X 400); **(b).** Dermal elastins and matrix protein degradation characterise disease-induced animals showing photoaged skin, the presence of acanthosis (line), spongiosis (arrow), and congestion in the dermis (arrowhead). (H. and E. X 400). **(c).** Animals treated with a piperine-loaded conventional gel of extract showed comparatively less compact collagen material in the dermis and a smaller population of fibroblasts. (H. and E.X400). **(d).** Animals treated with piperine loaded those gel formulations, showing normal epidermis and Dermis with Fewer collagen fibres in the dermis compared to the disease. (H. and E.X400), **(e).** Animal treated with marketed formulation showing dermis, few collagen fibres in the dermis (H. and E.X400).

and lipid. Morphological characterisation of prepared ethosomes was done by TEM, and Figure 1 showed that the ethosomes vesicles had spherical shapes and smooth surfaces. Formulations were evaluated for vesicle size, PDI, zeta potential, and entrapment efficiency. Zeta potential is the difference between the surfaces of a solid particle immersed in a conducting liquid. The stability of the ethosomal formulation can be determined from the zeta potential value. Zeta potential ranged from -26.33 to -51.48 mV (Table 1).The size of ethosomes prepared was found to be in an appropriate nano-size range between 128.2±1.11 nm to 312.6±1.06 nm. The literature suggests that vesicles below 300 nm can carry their drug into the deep layer of the skin. PDI indicates

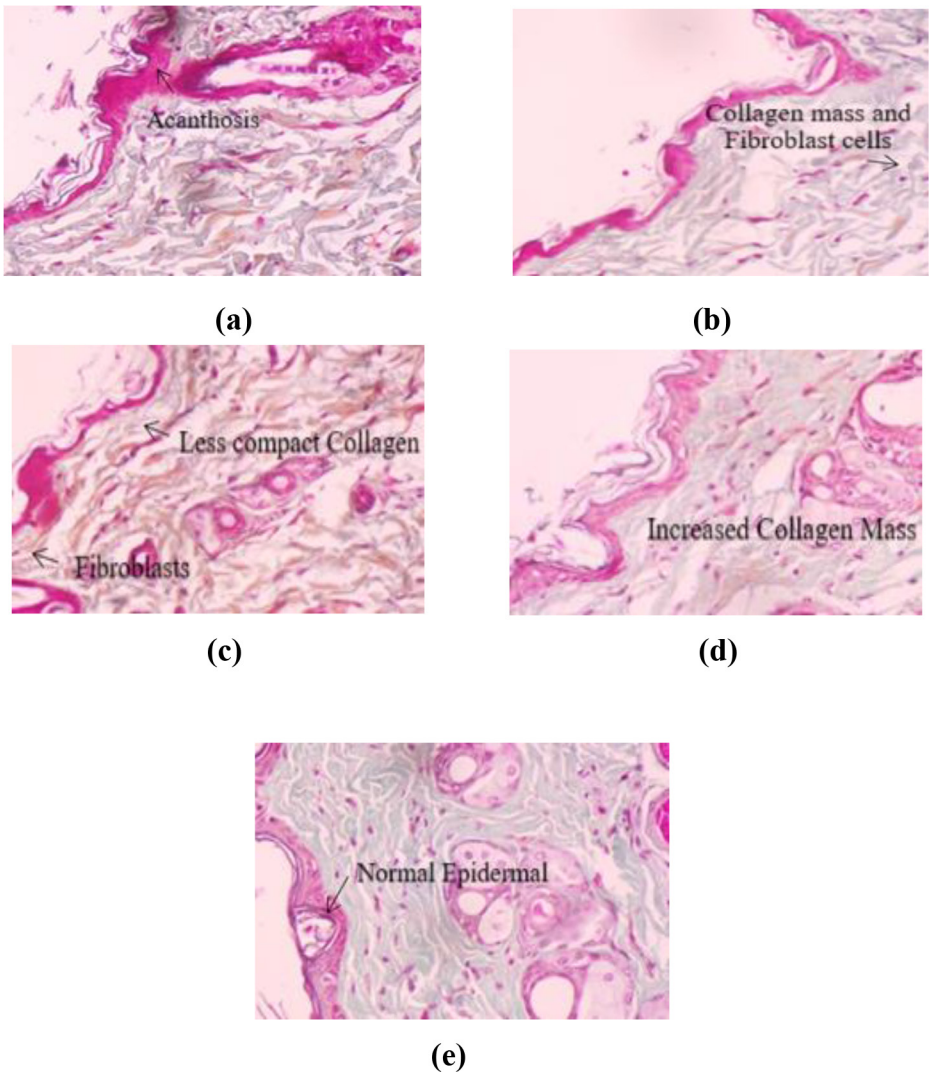


Figure 7. **(a).** Normal Control animal showing (a straight line) (i.e., thickened prickle cell layer) in the epidermis. (H. and E.X400), **(b).** Disease-induced animals show increased obedience in the dermis and neutrophils, indicating chronic changes. (H. and E. X 400), **(c).** Animals treated with a conventional piperine gel showed comparatively less compact collagen material in the dermis and a smaller population than those with the disease. (H. and E.X400), **(d).** Animals treated with piperine-loaded ethosomal gel showed increased collagen mass, and fibroblast cells were abundant in the dermis along with neutrophils, indicating chronic changes and mild acanthosis compared to the disease. (H.and E.X400) and **(e).** Animals treated with the marketed formulation show normal epidermal thickness and congestion (arrow) in the dermis. (H. and E.X400).

the width of the particle size distribution. In an ideal scenario, PDI value as zero indicates theoretically perfect monodisperse distribution, and PDI>0.5 indicates a wider size distribution. Our results revealed the distribution ranging from 0.107±1.21 to 0.322±1.32, confirming a narrow size distribution. Next, the entrapment of piperine in the ethosomal vesicles was evaluated. Entrapment efficiency reflects the percentage of the total added drug successfully entrapped within the ethosomal vesicles, serving as a critical quality attribute that influences the ethosome drug-carrying capacity. The entrapment efficiency was quantified for all ethosomal formulations. A direct proportionality was observed between the entrapment efficiency of drug-loaded ethosomes and the concentrations of soy Phosphatidylcholine (PC) and ethanol. The entrapment efficiency values ranged from 59.00 ± 0.32% to 94.00 ± 1.54% (mean ± standard deviation). Overall, high EE resulted from piperine's high solubility in ethanol (used to prepare ethosomes). After comparing the results of

entrapment efficiency, zeta potential, PDI, and vesicle size, formulations F-1, F-3, F-5, and F-6 were selected for *in vitro* drug permeation.

The percentage release was decreased with increasing amounts of lipid in ethosomes, though increasing the alcohol concentration somewhat increases the release. The observed increase in per cent release with a higher amount of alcohol could be due to increased fluidity of the bilayer membrane with increasing concentration of alcohol. Drug release profiling serves two important functions in formulation development. Firstly, it helps optimise the delivery system to achieve the desired therapeutic effects, and secondly, it helps ensure consistency and uniformity of the final product.

In vitro, release data were subjected to a kinetics study according to zero-order, first-order, and Higuchi Kinetics equations to determine the release mechanism. The R2 values of different formulations were higher in zero-order and first-order. Therefore, the formulations that follow first-order kinetics imply controlled and slow release by diffusion as proposed by the first order, which is non-Fickian diffusion and best for transdermal formulations. Figure 2 shows the release graph pattern of the four best-fitted formulations (F-1, F-3, F-5, F-6) and hydroethanolic solution, which makes it evident that F-5 shows the best release pattern. Permeation Data Analysis suggested that systems that obey zero-order release are ideal for transdermal extract delivery because they constantly release extracts over an extended period and reflect an improved therapeutic index.

The skin permeation ability of the probe-loaded ethosomal system – F5 was visualised employing CLSM, and the intensity of probe-entrapped lipid vesicles was found to be 16.36 (at 30–40 µm), whereas that of the hydroethanolic solution was 9.4863. CLSM data demonstrated that optimised ethosomal batch has ability to permeate deeper layers of the skin.

Batch F-1, F-3, F-5, and F-6 were lyophilised and incorporated into a 1% Carbopol gel base, recoded as GF-1, GF-3, GF-5, and GF-6, and characterised based on their colour, appearance, spreadability, viscosity, drug content, pH, and stability. The tests used for the characterisation of ethosomal gels. The optimised gel GF-5 was then used for further animal studies. The animal study was performed by inducing wrinkles on the dorsal skin of mice through UV-B exposure for 30 days. When UV-B radiations are used to induce wrinkles in mice, the subjected dorsal skin undergoes deformation owing to the degeneration of collagen and elastin fibres. In this case, the ensuing photoaging was treated with three topical gels: a conventional gel, an ethosomal gel – GF 5, and a marketed gel (Himalayan Anti-wrinkles Cream). After 21 days of continuous treatment, the skin was excised and tested through histopathological examination. This is essentially done to monitor the comparative changes that the skin undergoes in response to the treatment given. After a definite period, when the skin was evaluated, the results showed positive effects of the piperine-loaded ethosomal gel against photoaging. A decrease in wrinkles can be seen in Figure 5d, proving the efficacy of the locked formulation in reducing UV-B-induced wrinkles.

The histopathological studies provide valuable insights into photo-aged skin's structural and cellular changes. This can help us understand the changes in photo-aged skin and treatment-receiving skin. MT staining to study the changes in collagen mass, epidermal thickness, elastin fibers, and fibroblasts. The control mice group showed normal epidermis and dermal structure, while in the disease-induced group, the photoaged skin was characterised by dermal elastins and matrix protein degradation and an additional presence of acanthosis and spongiosis. The animal group treated with the conventional ethosomal gel showed comparatively less compact collagen material in the dermis, and a lower population of fibroblasts, and the animal group that received the marketed formulation showed normal epidermal thickness and congestion in the dermis, as shown in Figure 4. Compared to the former four groups, the animals treated with formulated piperine-loaded ethosomal gel showed increased collagen mass, and the fibroblast cells were obedient in the dermis along with neutrophils, indicating chronic changes and only mild acanthosis was observed. All these results show skin-ageing improvement in mice skin through the transdermal application of our piperine-loaded ethosomal gel formulation.

11. Conclusion

The UV-B radiation has increased the overall population of people who face premature skin aging.

This extrinsic factor sets in before the intrinsic skin aging accelerates and starts causing wrinkles through reduced collagen fibers, fibroblasts, and elastin fibers. The novel vesicular system – ethosomes was used to study and develop an innovative piperine-loaded transdermal gel formulation that could improve our active bioavailability and stability, and the overall health of photo-aged skin. The developed formulation successfully improved the state of the wrinkles induced externally through UV-B radiation. This formulation can act as a new approach to resolve skin-ageing issues and reduce the appearance of wrinkles in UV-B-induced photo-aged skin.

12. Author Contribution

Conceptualization and Supervision – Dr. Nimisha, Writing; methodology- Deepti and Dr.Nimisha; editing and Co supervision - Dr. Neeraj Mishra; Animal Activity- Dr. S P Singh and Dr. Ankur Srivastava. All authors have read and agreed to the published version of the manuscript.

13. References

1. Som PM, Laitman JT, Mak K. Embryology and anatomy of the skin, its appendages, and physiologic changes in the head and neck. Neurographics. 2017; 7(5):390-415. https://doi.org/10.3174/ng.9170210
2. Chambers ES, Vukmanovic-Stejic M. Skin barrier immunity and aging. Immunology. 2020; 160(2):116-125. https://doi.org/10.1111/imm.13152 PMid:31709535 PMCid:PMC7218662
3. Manosroi A, Jantrawut P, Akihisa T, Manosroi W, Manosroi J. *In vitro* and *in vivo* skin anti-aging evaluation of gel containing niosomes loaded with a semi-purified fraction containing gallic acid from *Terminalia chebula* galls. Pharmaceut Bio. 2011; 49(11):1190-1203. https://doi.org/10.3109/13880209.2011.576347 PMid:22014267
4. Strnadova K, Sandera V, Dvorankova B, Kodet O, Duskova M, Smetana K, *et al*. Skin aging: The dermal perspective. Clinic Dermatol. 2019; 37(4):326-335. https://doi.org/10.1016/j.clindermatol.2019.04.005 PMid:31345320
5. Freitas-Rodriguez S, Folgueras AR, Lopez-Otin C. The role of matrix metalloproteinases in aging: Tissue remodelling and beyond. Biochim Biophys Acta. 2017; 1864(11):2015-2025. https://doi.org/10.1016/j.bbamcr.2017.05.007 PMid:28499917
6. Rittié L, Fisher GJ. UV-light-induced signal cascades and skin aging. Ageing Res Rev. 2002; 1(4):705-720. https://doi.org/10.1016/S1568-1637(02)00024-7 PMid:12208239
7. Debacq-Chainiaux F, Leduc C, Verbeke A, Toussaint O. UV, stress and aging. Dermato-endocrinol. 2012; 4(3):236-240. https://doi.org/10.4161/derm.23652 PMid:23467762 PMCid:PMC3583883
8. Agarwal P, Alok S, Fatima A, Verma A. Current scenario of herbal technology worldwide: An overview. Int J Pharm Sci Res. 2013; 4(11):4105.
9. Dwivedi D, Mishra N, Singh SP, Shukla AK. Performance evaluation of *Bacopa monneri*-loaded ethosomes for topical delivery. J Appl Nat Sci. 2024; 16(3). https://doi.org/10.31018/jans.v16i3.5435
10. Haq IU, Imran M, Nadeem M, Tufail T, Gondal TA, Mubarak MS. Piperine: A review of its biological effects. Phytother Res. 2021; 35(2):680-700. https://doi.org/10.1002/ptr.6855 PMid:32929825
11. Derosa G, Maffioli P, Sahebkar A. Piperine and its role in chronic diseases. Anti-inflammatory nutraceuticals and chronic diseases; 2016. p. 173-184. https://doi.org/10.1007/978-3-319-41334-1_8 PMid:27671817
12. Gupta, Rishabh, and Nimisha Srivastava. "Nanoformulations Enabled Possible Solutions for the Management of Psoriasis." Current Cosmetic Science 1, no. 2 (2022): e230622206307 https://doi.org/10.2174/2666779701666220623085521
13. Nainwal N, Jawla S, Singh R, Saharan VA. Transdermal applications of ethosomes – A detailed review. J Liposome Res. 2019; 29(2):103-113. https://doi.org/10.1080/08982104.2018.1517160 PMid:30156120
14. Gupta M, Chauhan DN, Sharma V, Chauhan NS, editors. Novel drug delivery systems for phytoconstituents. CRC Press; 2019. https://doi.org/10.1201/9781351057639
15. Emanet M, Ciofani G. Ethosomes as promising transdermal delivery systems of natural-derived active compounds. Adv NanoBiomed Res. 2023; 3(10):2300020. https://doi.org/10.1002/anbr.202300020
16. Thakur N, Jain P, Jain V. Formulation development and evaluation of transferosomal gel. J Drug Deliv Ther. 2018; 8(5):168-177. https://doi.org/10.22270/jddt.v8i5.1826
17. Sanchez II. G3BP1-positive stress granule pathology in brains of Huntington's disease mice and human patients and a potential role for extracellular vesicle-derived miRNA regulation. University of California, Irvine; 2020.
18. Yue PF, Lu XY, Zhang ZZ, Yuan HL, Zhu WF, Zheng Q, *et al*. The study on the entrapment efficiency and in vitro release of puerarin submicron emulsion. AAPS Pharmscitech. 2009; 10:376-383. https://doi.org/10.1208/s12249-009-9216-3 PMid:19381837 PMCid:PMC2690779
19. Mousa IA, Hammady TM, Gad S, Zaitone SA, El-Sherbiny M, Sayed OM. Formulation and characterization of metformin-loaded ethosomes for topical application to experimentally induced skin cancer in mice. Pharmaceuticals. 2022; 15(6):657. https://doi.org/10.3390/ph15060657 PMid:35745575 PMCid:PMC9227071

20. Zhai Y, Xu R, Wang Y, Liu J, Wang Z, Zhai G. Ethosomes for skin delivery of ropivacaine: Preparation, characterization and *ex vivo* penetration properties. J Liposome Res. 2015; 25(4):316-324. https://doi.org/10.3109/08982104.2014.999686 PMid:25625544
21. Venugopal V, Goh R, Ping TY, Jin TJ. Formulation development and characterization of tea tree oil-loaded ethosomes. Indones J Pharm. 2016; 27(1):44. https://doi.org/10.14499/indonesianjpharm27iss1pp44
22. Chen JG, LaI W, JIANG Y. Preparation of curcumin ethosomes. Afr J Pharm Pharmacol. 2013; 7:2246-2251. https://doi.org/10.5897/AJPP12.435
23. El-Hashemy HA. Design, formulation, and optimization of topical ethosomes using full factorial design: *In vitro* and *ex vivo* characterization. J Liposome Res. 2022; 32(1):74-82. https://doi.org/10.1080/08982104.2021.1955925 PMid:34697998
24. Lin H, Lin L, Choi Y, Michniak-Kohn B. Development and *in-vitro* evaluation of co-loaded berberine chloride and evodiamine ethosomes for treatment of melanoma. Int J Pharm. 2020; 581:119278. https://doi.org/10.1016/j.ijpharm.2020.119278 PMid:32229284
25. Sguizzato M, Ferrara F, Hallan SS, Baldisserotto A, Drechsler M, Malatesta M, *et al*. Ethosomes and transethosomes for mangiferin transdermal delivery. Antioxidants. 2021; 10(5):768. https://doi.org/10.3390/antiox10050768 PMid:34066018 PMCid:PMC8150765
26. Pathan IB, Jaware BP, Shelke S, Ambekar W. Curcumin loaded ethosomes for transdermal application: Formulation, optimization, *in vitro* and *in vivo* study. J Drug Deliv Sci Technol. 2018; 44:49-57. https://doi.org/10.1016/j.jddst.2017.11.005
27. David SR, Hui MS, Pin CF, Ci FY, Rajabalaya R. Formulation and in vitro evaluation of ethosomes as a vesicular carrier for enhanced topical delivery of isotretinoin. Int J Drug Deliv. 2013; 5(1):28.
28. Bisht D, Verma D, Mirza MA, Anwer MK, Iqbal Z. Development of ethosomal gel of ranolazine for improved topical delivery: *In vitro* and *ex vivo* evaluation. Journal of molecular liquids. 2017; 225:475-481. https://doi.org/10.1016/j.molliq.2016.11.114
29. Srivastava, Nimisha, Zeeshan Fatima, Chanchal D. Kaur, and Dilshad A. Rizvi. "Berberine chloride dihydrate enthused nanovesicles for the management of dermatitis nanovesicles for dermatitis." *Nanoscience and Nanotechnology-Asia* 11, no. 3 (2021): 300-313 https://doi.org/10.2174/2210681210666200313123550
30. Ramadon D, Wirarti GA, Anwar E. Novel transdermal ethosomal gel containing green tea (*Camellia sinensis* L. Kuntze) leaves extract: Formulation and *in vitro* penetration study. J Young Pharm. 2017; 9(3):336. https://doi.org/10.5530/jyp.2017.9.67
31. Kumar P, Sharma DK, Ashawat MS. Topical creams of piperine loaded lipid nanocarriers for management of atopic dermatitis: Development, characterization, and in vivo investigation using BALB/c mice model. J Liposome Res. 2022; 32(1):62-73. https://doi.org/10.1080/08982104.2021.1880436 PMid:33944670
32. Indora N, Kaushik D. Design, development, and evaluation of ethosomal gel of fluconazole for topical fungal infection. Int J Eng Sci Invention Res Dev. 2015; 1(8):280-306.
33. Garg NK, Tyagi RK, Singh B, Sharma G, Nirbhavane P, Kushwah V, *et al*. Nanostructured lipid carrier mediates effective delivery of methotrexate to induce apoptosis of rheumatoid arthritis via NF-κB and FOXO1. Int J Pharm. 2016; 499(1-2):301-320. https://doi.org/10.1016/j.ijpharm.2015.12.061 PMid:26768725
34. Fathalla D, Youssef EM, Soliman GM. Liposomal and ethosomal gels for the topical delivery of anthralin: Preparation, comparative evaluation and clinical assessment in psoriatic patients. Pharmaceutics. 2020; 12(5):446. https://doi.org/10.3390/pharmaceutics12050446 PMid:32403379 PMCid:PMC7285224
35. Thomas MA. Formulation and evaluation of ethosomal gel of tazarotene for topical delivery. Asian J Pharm. 2019; 13(01).
36. Chettupalli AK, Ajmera S, Amarachinta PR, Manda RM, Jadi RK. Quality by design approach for preparation, characterization, and statistical optimization of naproxen sodium-loaded ethosomes via transdermal route. Curr Bioact Compd. 2023; 19(10):79-98. https://doi.org/10.2174/1573407219666230606142116
37. Sharma T, Thakur S, Kaur M, Singh A, Jain SK. Novel hyaluronic acid ethosomes-based gel formulation for topical use with reduced toxicity, better skin permeation, deposition, and improved pharmacodynamics. J Liposome Res. 2023; 33(2):129-143. https://doi.org/10.1080/08982104.2022.2087675 PMid:35730480
38. Arora D, Khurana B, Nanda S. Statistical development and *in vivo* evaluation of resveratrol-loaded topical gel containing deformable vesicles for a significant reduction in photo-induced skin aging and oxidative stress. Drug Dev Ind Pharm. 2020; 46(11):1898-1910. https://doi.org/10.1080/03639045.2020.1826507 PMid:32962434
39. Lin M, Liu X, Wang X, Chen Y, Zhang Y, Xu J, *et al*. A comparative study of skin changes in different species of mice in chronic photoaging models. Int J Mol Sci. 2023; 24(13):10812. https://doi.org/10.3390/ijms241310812 PMid:37445996 PMCid:PMC10341798
40. Yue KO, Yan GU. Construction and evaluation of skin photoaging mouse model. Lab Animal Comp Med. 2021; 41(2):116.
41. Tong T, Geng R, Kang SG, Li X, Huang K. Revitalizing photoaging skin through Eugenol in UVB-exposed

hairless mice: Mechanistic insights from integrated multi-omics. Antioxidants. 2024; 13(2):168. https://doi.org/10.3390/antiox13020168 PMid:38397766 PMCid:PMC10886361

42. Maqbool N, Ali Z, Batool S, ur Rehman M, Alamri AH, Al Fatease A, *et al*. Improved wound care via novel dextran and boric acid loaded wound healing gel in excision mice wound model. J Drug Deliv Sci Technol. 2025; 105:106586. https://doi.org/10.1016/j.jddst.2024.106586
43. Nwankwo JA, Liu W, Guo X, Lin Y, Hussain M, Khan I, *et al*. Microemulsion gel systems: Formulation, stability studies, biopolymer interactions, and functionality in food product development. Compr Rev Food Sci Food Saf. 2025; 24(2):e70110. https://doi.org/10.1111/1541-4337.70110 PMid:39898912
44. Imokawa G, Ishida K. Biological mechanisms underlying the ultraviolet radiation-induced formation of skin wrinkling and sagging I: Reduced skin elasticity, highly associated with enhanced dermal elastase activity, triggers wrinkling and sagging. Int J Mol Sci. 2015; 16(4):7753-7775. https://doi.org/10.3390/ijms16047753 PMid:25856675 PMCid:PMC4425048
45. El-Domyati M, Attia S, Saleh F, Brown D, Birk DE, Gasparro F, *et al*. Intrinsic aging vs. photoaging: A comparative histopathological, immunohistochemical, and ultrastructural study of skin. Exp Dermatol. 2002; 11(5):398-405. https://doi.org/10.1034/j.1600-0625.2002.110502.x PMid:12366692